Supplementary Figures

IL27 signaling serves as an immunologic checkpoint for innate cytotoxic cells to promote hepatocellular carcinoma

Turan Aghayev[1,#], Aleksandra M. Mazitova[1, 2,#], Jennifer R. Fang[3,#], Iuliia O. Peshkova[1], Matthew Rausch[4], Manhsin Hung[5,6], Kerry F. White[4], Ricard Masia[4], Elizaveta K. Titerina[1], Aliia R. Fatkhullina[1], Isabelle Cousineau[7], Simon Turcotte[7], Dmitry Zhigarev[1], Anastasiia Marchenko[2], Svetlana Khoziainova[2], Petr Makhov[8], Yin Fei Tan[9], Andrew V. Kossenkov[10], David L.Wiest[1], John Stagg[7], Xin Wei Wang[5,6], Kerry S. Campbell[1], Amiran K. Dzutsev[3], Giorgio Trinchieri[3], Jonathan A. Hill[4], Sergei I. Grivennikov[2, 11,*], Ekaterina K. Koltsova[1, 2, 12,*]

[1] Blood Cell Development and Function Program, Fox Chase Cancer Center, Philadelphia, PA 19111, USA
[2] Cedars-Sinai Medical Center, Cedars-Sinai Cancer Institute, Department of Medicine, Department of Biomedical Sciences 8700 Beverly Blvd, Los Angeles, CA, 90048
[3] Laboratory of Integrative Cancer Immunology, Center for Cancer Research, National Cancer Institute, National Institutes of Health, Bethesda, MD, USA, 20892
[4] Surface Oncology Inc., 50 Hampshire St. Cambridge, MA, 02139
[5] Laboratory of Human Carcinogenesis, Center for Cancer Research, National Cancer Institute, National Institutes of Health, Bethesda, MD, USA, 20892
[6] Liver Cancer Program, Center for Cancer Research, National Cancer Institute, National Institutes of Health, Bethesda, MD, USA, 20892
[7] Centre Hospitalier de l'Université de Montréal Research Center, Montreal, Quebec, Canada
[8] Molecular Therapeutics Program, Fox Chase Cancer Center, Philadelphia, PA, 19111, USA
[9] Genomics Facility, Fox Chase Cancer Center, Philadelphia, PA 19111, USA
[10] Bioinformatics Facility, The Wistar Institute, Philadelphia, PA 19104, USA
[11] Cancer Prevention and Control Program, Fox Chase Cancer Center, Philadelphia, PA, 19111, USA
[12] Corresponding and Lead Author, contact: Ekaterina Koltsova, MD, PhD, Department of Medicine, Department of Biomedical Sciences, Cedars-Sinai Medical Center, 8700 Beverly Blvd, Los Angeles, CA, 90048, USA., phone: +1-310-423-8899, E-mail: Ekaterina.Koltsova@cshs.org

# these first authors equally contributed to this work
• these senior authors equally contributed to this work

Running title: IL-27R suppresses anti-cancer innate cytotoxic cells in HCC

K.F.W, M.R., R.M. and J.A.H. are either current or former employees and stockholders of Surface Oncology, Inc. J.S. received research funding and is a scientific advisor and stockholder of Surface Oncology. E.K.K. received research funding from Surface Oncology to investigate IL-27 blockade in HCC. J.A.H., M.R., K.F.W. and E.K.K. are inventors on pending patent applications associated with the topic presented in this article. Other authors declare no potential conflicts of interest.

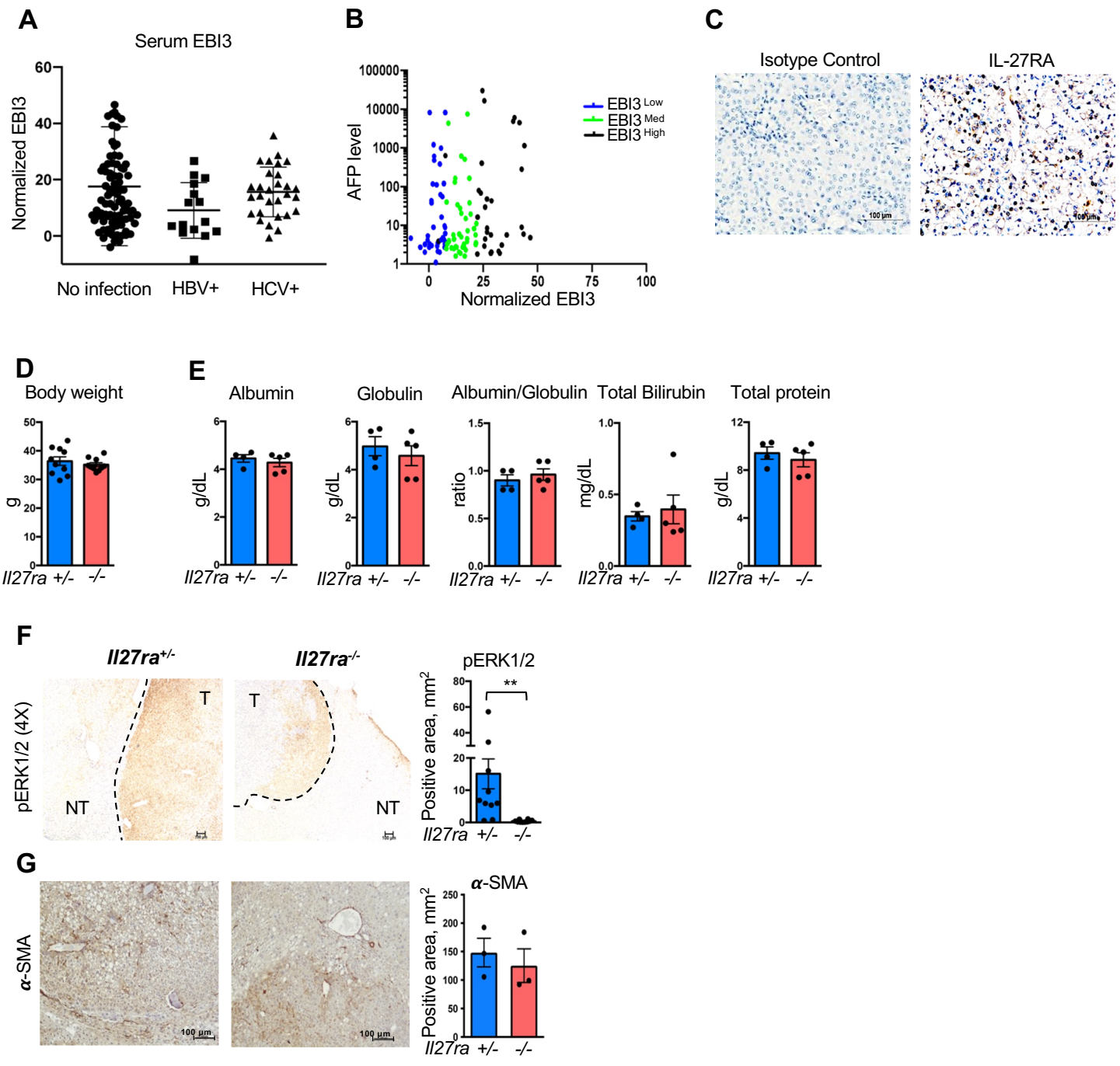

Supplementary Figure S1. IL27R signaling is implicated in the regulation of HCC.
A, ELISA analysis of serum IL27EBI3 levels in HCC patients grouped by viral infections status. HBV^+-hepatitis B virus positive; HCV^+-hepatitis C virus positive. Note that HCV^+ patients showed higher serum EBI3 levels compared to HBV^+ patients ($p=0.03$), however no differences were observed when comparing with the "no infection" patients. **B,** No correlation between serum AFP and EBI3 levels in the CHUM HCC patient cohort. **C,** Representative images of IHC staining for IL-27RA expression in human HCC. **D,** Body weight of DEN-injected tumor-bearing *Il27ra*$^{+/-}$ (n=10) and *Il27ra*$^{-/-}$ (n=10) male mice. **E,** Circulating proteins in serum of DEN-injected tumor-bearing *Il27ra*$^{+/-}$ (n=4) and *Il27ra*$^{-/-}$ (n=5) male mice. **F,G,** Representative images and quantification of IHC staining for p-ERK1/2 (**F**) and α-SMA (**G**) on sections of HCC-bearing livers from DEN-injected *Il27ra*$^{+/-}$ (n=3-12) and *Il27ra*$^{-/-}$ (n=3-10) mice. Data are mean ± SEM. ** $p<0.01$.

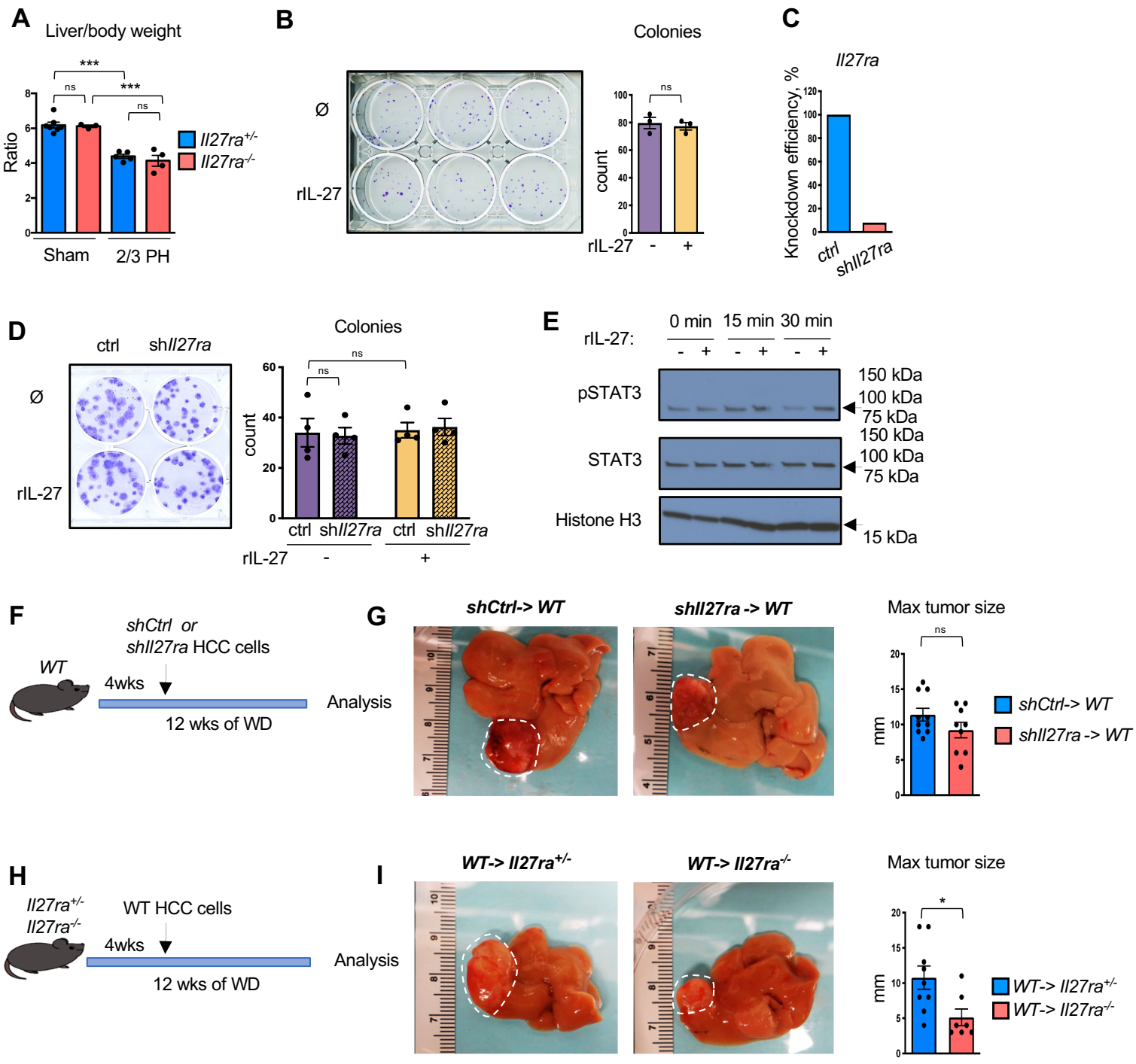

Supplementary Figure S2. IL27R on hepatocytes or HCC cells does not affect cell proliferation.
A, Liver to body weight ratio of *Il27ra*$^{+/-}$ (n=7) and *Il27ra*$^{-/-}$ (n=3) and *Il27ra*$^{+/-}$ (n=5) and *Il27ra*$^{-/-}$ (n=4) male mice subjected to 2/3 partial hepatectomy (PH) or sham surgery. **B,** Representative image and quantification of the colonies of DEN-derived HCC cells stimulated *in vitro* with rIL27. **C,** Efficiency of *Il27ra* knockdown by shRNA as determined by Q-RT-PCR. **D,** Representative image and quantification of the colonies of DEN-derived HCC cells with or without knockdown of *Il27ra,* which were stimulated *in vitro* with rIL27. Data are mean ± SEM from at least 2 independent experiments. **E,** Western blot analysis of phospho-STAT3 and STAT3 protein expression in DEN-derived HCC cells treated with rIL27 *in vitro* for 0, 15 min or 30 min. **F,** Scheme of experiment. HCC cells with or without knockdown of *Il27ra* were orthotopically transplanted to livers of C57BL/6 mice fed with WD. **G** Macroscopic images of liver tumors and quantification of maximum tumor sizes. **H,** Scheme of experiment. IL27R sufficient HCC cells were orthotopically transplanted to livers of *Il27ra*$^{+/-}$ or *Il27ra*$^{-/-}$ mice fed with WD. **I,** Macroscopic images of liver tumors and quantification of maximum tumor sizes. Data are mean ± SEM from at least 3 independent experiments. ***p<0.001, *p<0.05. Tukey's multiple comparisons test **(A, D)**.

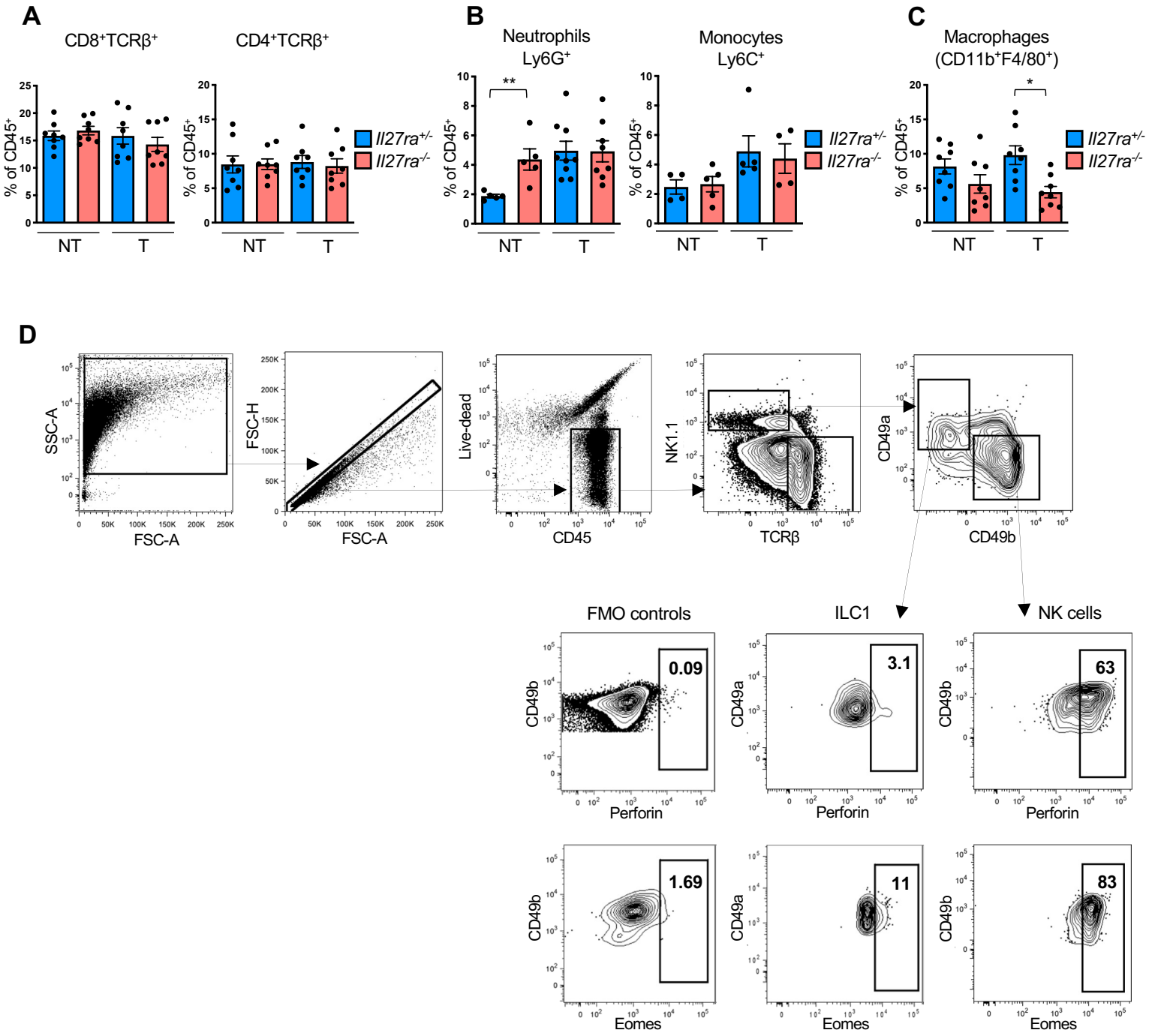

Supplementary Figure S3. The role of IL27R in the regulation of immune tumor microenvironment in HCC. FACS analysis of immune cells infiltrating non-tumor (NT) and tumor (T) tissues of DEN- treated *Il27ra*$^{+/-}$ and *Il27ra*$^{-/-}$ mice. Percentage of (**A**) CD8^{+}TCRβ^{+} and CD4^{+}TCRβ^{+} cells, (**B**) Ly6G^{+} (neutrophils) and Ly6C^{+} (inflammatory monocytes), (**C**) F4/80^{+} macrophages are shown (n=4-9). Data are mean ± SEM from at least 3 independent experiments from DEN injected, tumor bearing 10-month-old mice. **D,** Gating strategy to define and characterize NK versus ILC1 cells within NK1.1^{+} TCRβ^{-} population.

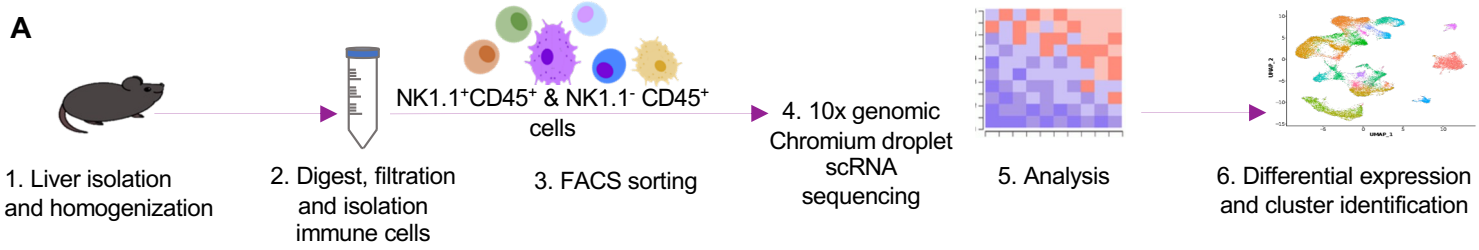

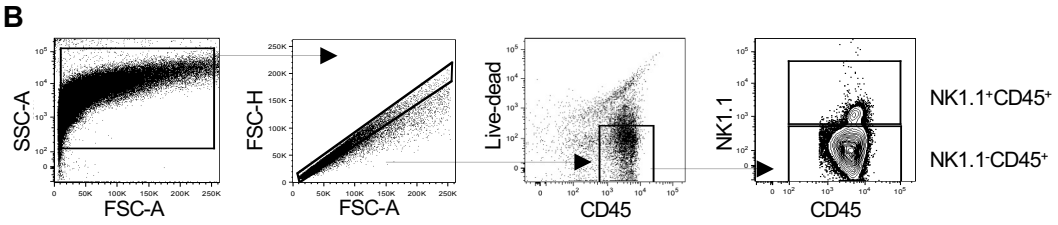

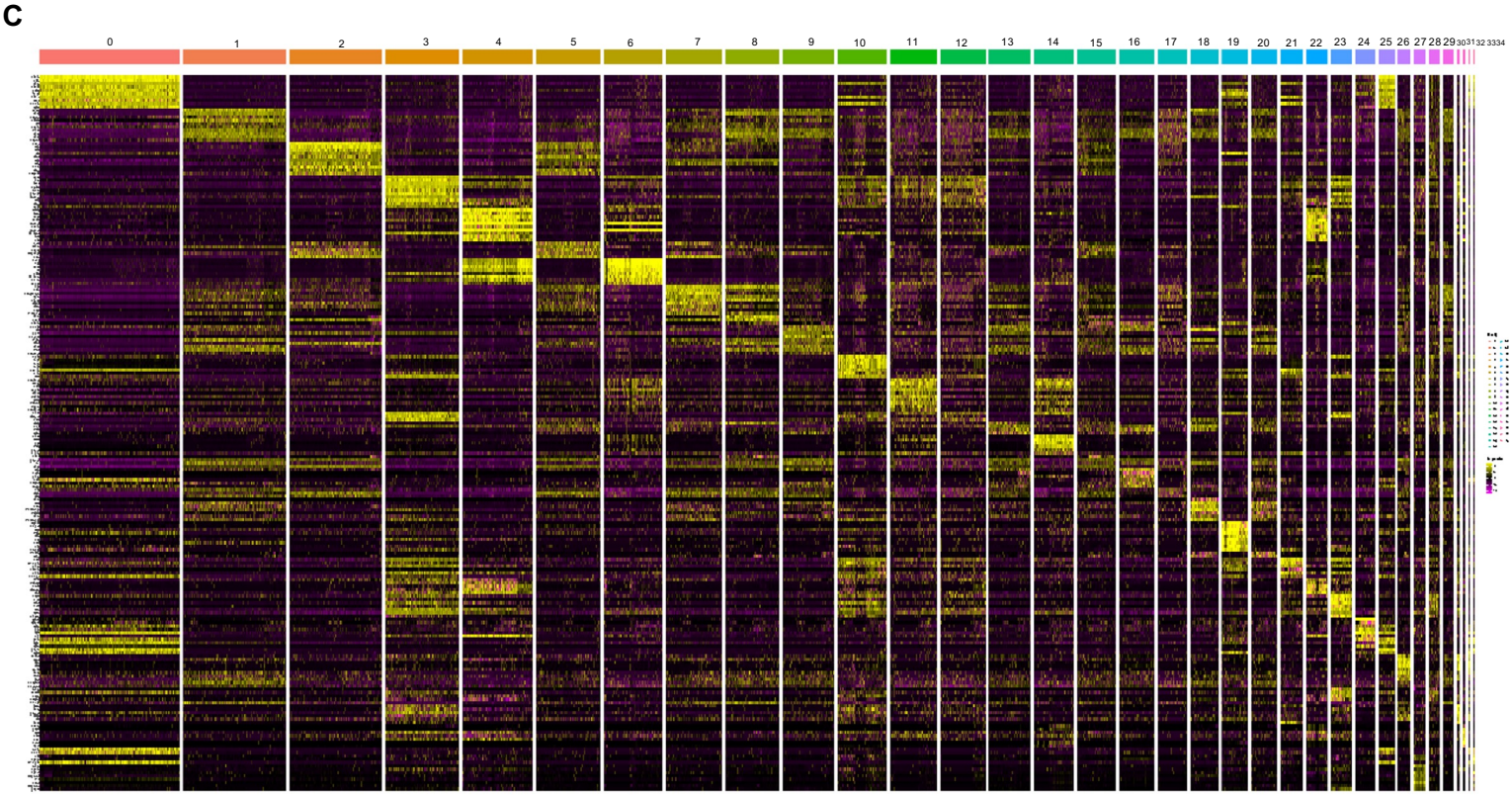

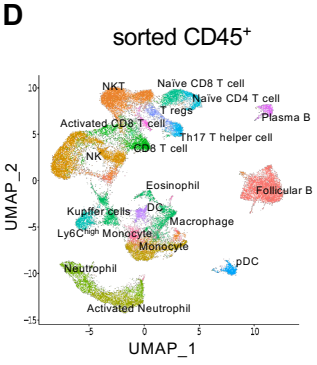

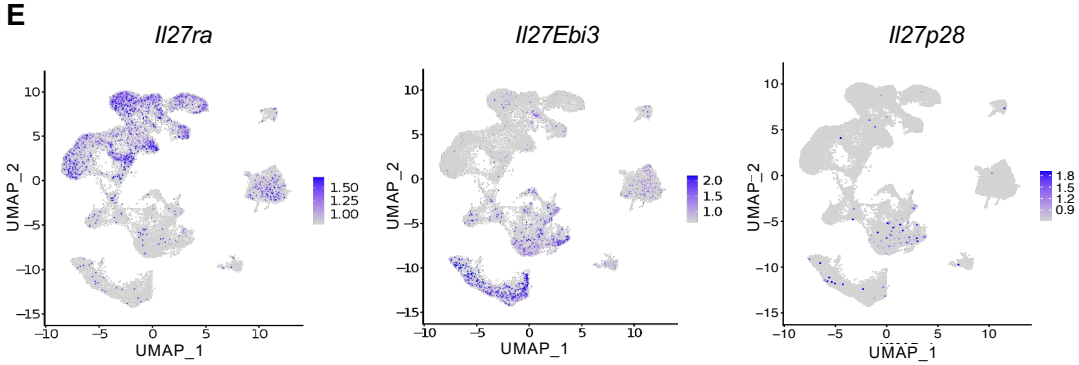

Supplementary Figure S4

Supplementary Figure S4. Single cell RNA sequencing analysis of HCC-infiltrating immune cells. **A,** Scheme of scRNA seq pipeline to analyze $CD45^+$ immune cells in non-tumor (NT) and tumor (T) tissues of DEN-treated *Il27ra*$^{+/-}$ and *Il27ra*$^{-/-}$ mice. **B,** Gating strategy for FACS sorting of $CD45^+NK1.1^+$ and $CD45^+NK1.1^-$ cells. **C,** Heatmap overview of significantly differentially expressed genes which define various clusters of $CD45^+$ cells using Seurat. **D,** UMAP plot of 41772 pooled mouse $CD45^+NK1.1^+$ and $CD45^+NK1.1^-$ cells isolated from NT and T tissues of DEN-treated *Il27ra*$^{+/-}$ and *Il27ra*$^{-/-}$ mice and subjected to 10x Genomics single cell droplet scRNA sequencing. Cluster analysis yields 34 distinct clusters and 19 immune cell types. **E,** UMAP plot shows cell type specific expression pattern for *Il27ra, Il27Ebi3, Il27p28* among clusters.

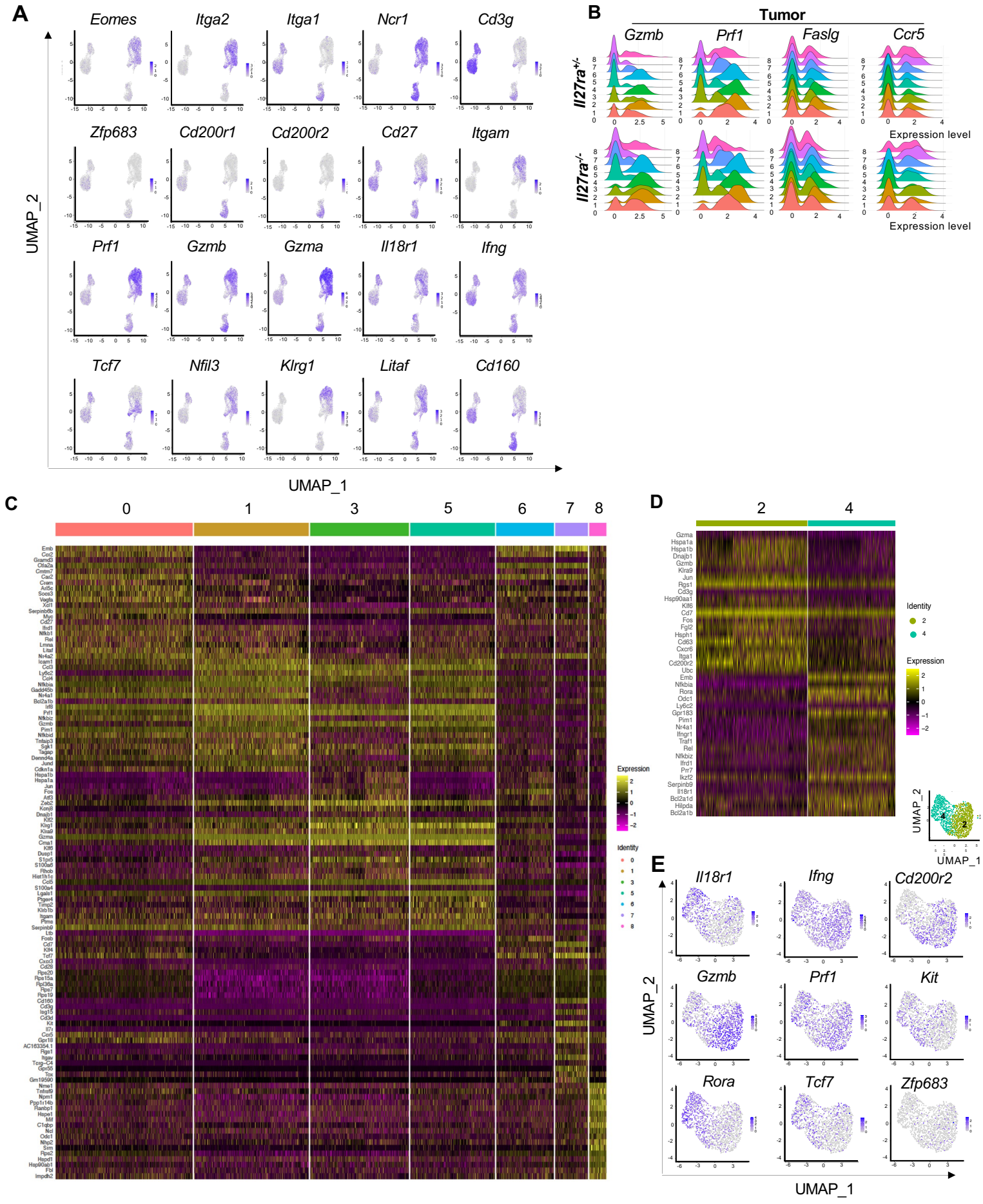

Supplementary Figure S5

Supplementary Figure S5. Single cell RNA sequencing analysis of NK1.1^{+} cells.
A, UMAP plots for selected genes for NK, ILC1 and NKT cells among sorted CD45^{+}NK1.1^{+} cells (see also Fig. 3C). **B,** Ridge plot visualization for the expression of selected cytotoxicity and recruitment markers among NK and ILC1 clusters. **C,D,** Heatmap of differentially expressed genes which define NK clusters **(C)** and ILC1 clusters **(D)** depicted on **Fig. 3F** and **3K**, respectively. **(E)** Selected UMAP feature plots showing RNA expression of additional cluster markers for ILC1 clusters.

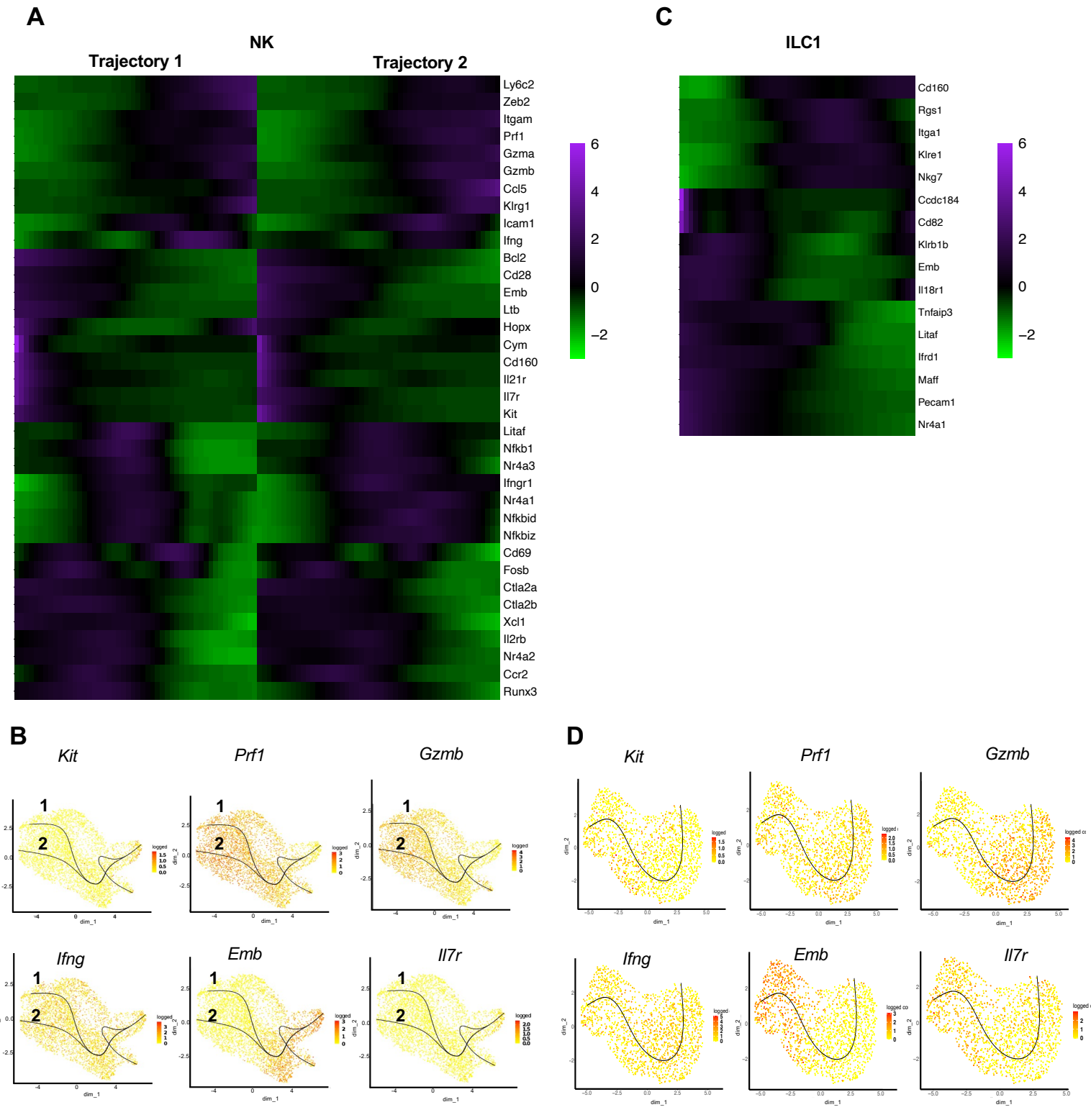

Supplementary Figure S6. Differential gene expression during NK and ILC1 differentiation regulated by IL27R. A, Heatmap of enriched genes for NK trajectories shown on **Fig 3F**. **B,** UMAP plots visualizing gene expression of selected genes along the trajectories of NK cell differentiation. **C,** Heatmap of enriched genes for ILC1 trajectory shown on **Fig 3K. D,** UMAP plots visualizing gene expression of selected genes along the trajectories ILC1 differentiation. Color indicates increased (violet) or decreased (green) expression.

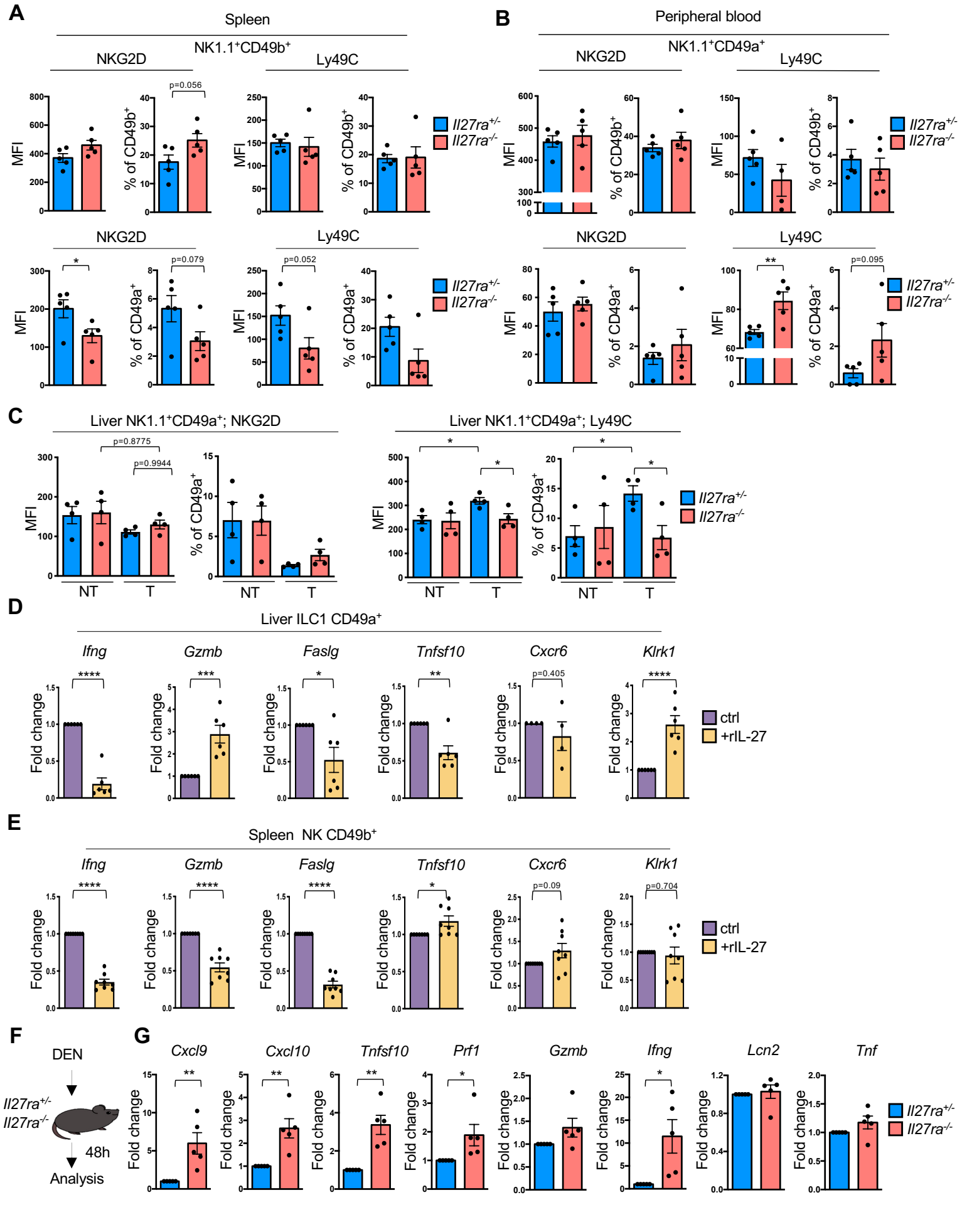

Supplementary Figure S7

Supplementary Figure S7. Role of IL27R signaling in the regulation of innate cytotoxic cells activity and response. Single cell suspensions of spleen, liver or peripheral blood from DEN-treated *Il27ra*$^{+/-}$ (n=4-5) and *Il27ra*$^{-/-}$ (n=4-5) 10-month-old mice were stained for Live/Dead, CD45, TCRβ, NK1.1, CD49a, CD49b, NKG2D, Ly49C and analyzed by FACS. Mean fluorescence intensity (MFI) and percentage of positive cells for NKG2D and Ly49C expression on NK1.1^{+}TCRβ^{-}CD49b^{+} NK and NK1.1^{+}TCRβ^{-}CD49a^{+} ILC1 cells in spleens (**A**) and peripheral blood (**B**)**. C,** MFI of expression for NKG2D and Ly49C and percentage of positive cells among NK1.1^{+} TCRβ^{-}CD49a^{+} liver ILC1 cells. **D,E,** Q-RT-PCR analysis of relative gene expression of cytotoxic genes in liver CD49a^{+} ILC1 cells (**D)** or splenic CD49b^{+} NK cells (**E**) stimulated *in vitro* with rIL27 (n=4-8). Gene expression was normalized to *Rpl32,* and then to the gene expression in control. Data are mean ± SEM from at least 3 independent experiments. **F,** Scheme of the experiment. 8-week-old *Il27ra*$^{+/-}$ and *Il27ra*$^{-/-}$ male mice were injected with 100 mg/kg of DEN. Inflammatory gene expression in livers was analyzed 48h later by Q-RT-PCR. **G,** Relative gene expression of chemokines, cytokines and cytotoxic molecules in livers of *Il27ra*$^{+/-}$ (n=5) and *Il27ra*$^{-/-}$ (n=5) male mice. Gene expression was first normalized to *Rpl32* then to gene expression in liver of *Il27ra*$^{+/-}$ mice. Data are mean ± SEM from at least 3 independent experiments. *p<0.05, **p<0.01, unpaired Student's t-test (two-tailed).

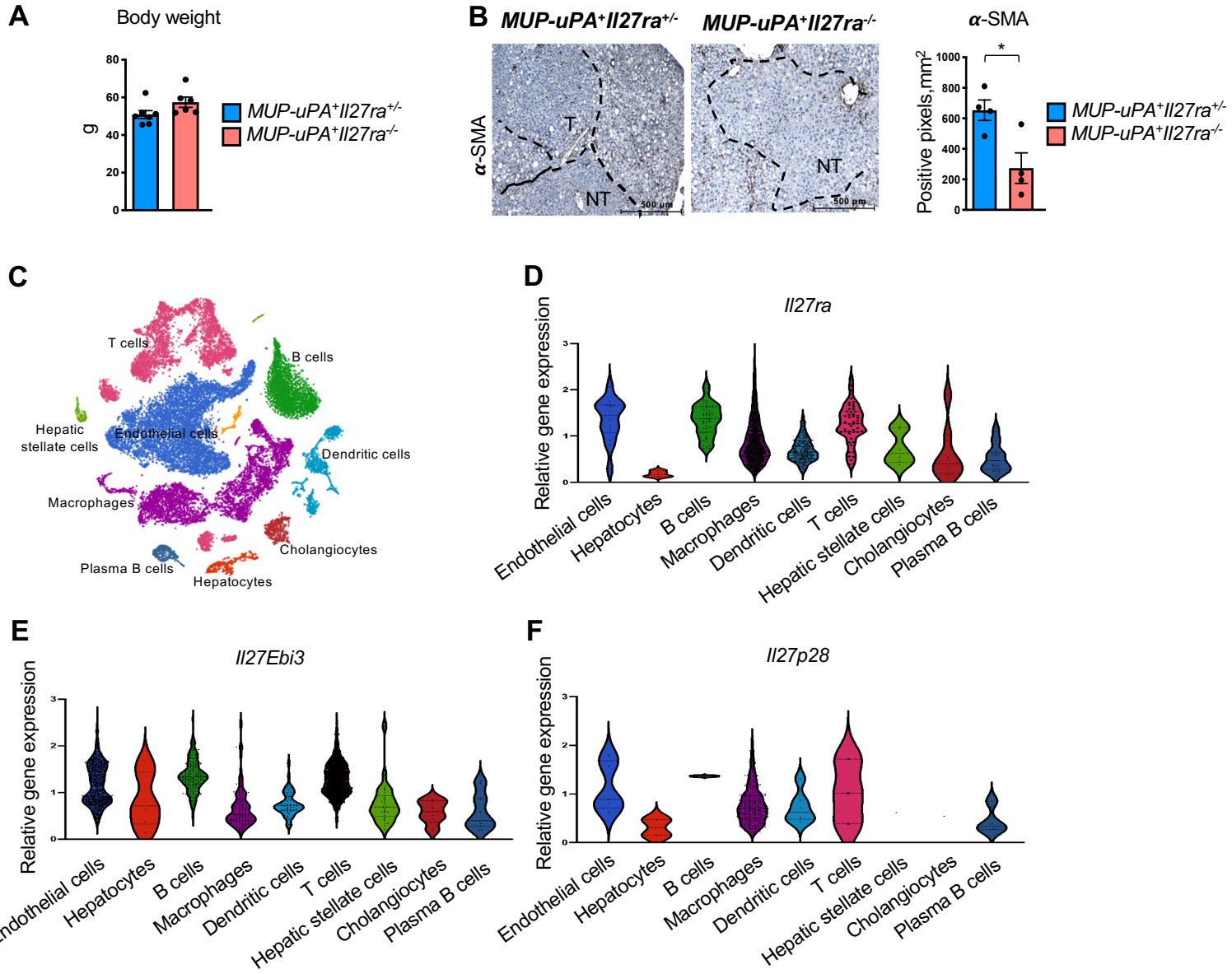

Supplementary Figure S8. IL27R in NASH and NASH-driven HCC.
A, Body weight of WD-fed tumor-bearing mice *MUP-uPA^{+}Il27ra$^{+/-}$* (n=7) and *MUP-uPA^{+}Il27ra$^{-/-}$* (n=6) male mice. **B,** Representative images and quantification of α-SMA staining of HCC sections from *MUP-uPA^{+} Il27ra$^{+/-}$* and *MUP-uPA^{+} Il27ra$^{-/-}$* mice (n=4). Data are mean ± SEM from at least 3 independent experiments. **C-F,** 10x Genomics-based platform single cell RNA sequencing of cells from livers of mice on regular or NASH-inducing diet (dataset GSE129516)(84). Analysis was performed using BBrowser software. **C**, UMAP plot representing cell clusterization. **D-F,** Violin plot representing cell type specific expression *of Il27ra, Il27Ebi3, Il27p28* in identified clusters.

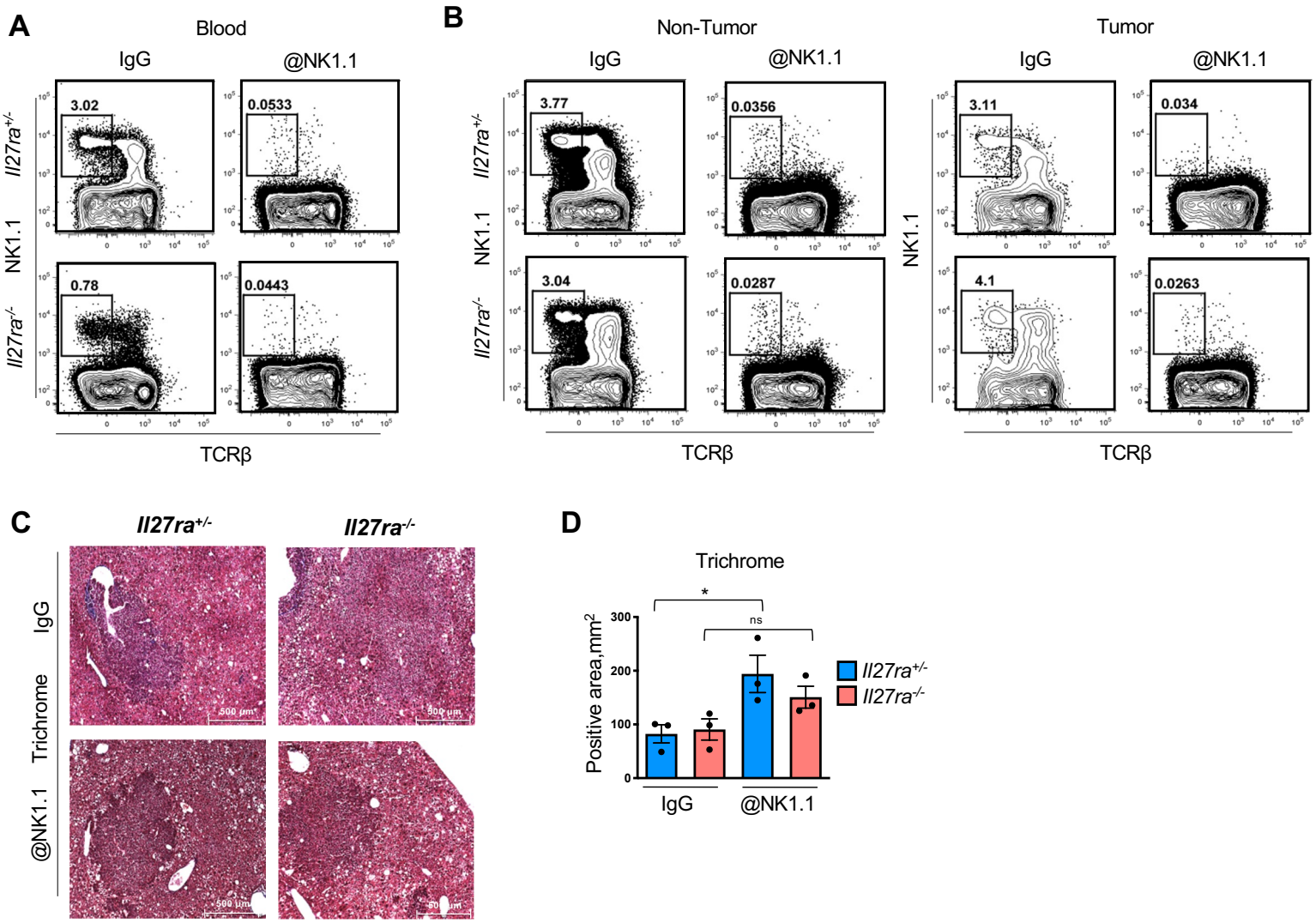

Supplementary Figure S9. Depletion of NK1.1 cells in DEN-driven HCC.
Representative FACS plots of NK cell depletion efficiency in blood (**A**) and non-tumor and tumor tissue (**B**) from DEN-driven tumor bearing *Il27ra*$^{+/-}$ and *Il27ra*$^{-/-}$ male mice which received anti-NK1.1 or isotype control antibody. Representative images (**C**) and quantification of fibrosis (**D**) as determined by Trichrome staining of liver sections from DEN-driven tumor bearing *Il27ra*$^{+/-}$ (n=3) and *Il27ra*$^{-/-}$ (n=3) mice received anti-NK1.1 or isotype control antibody.

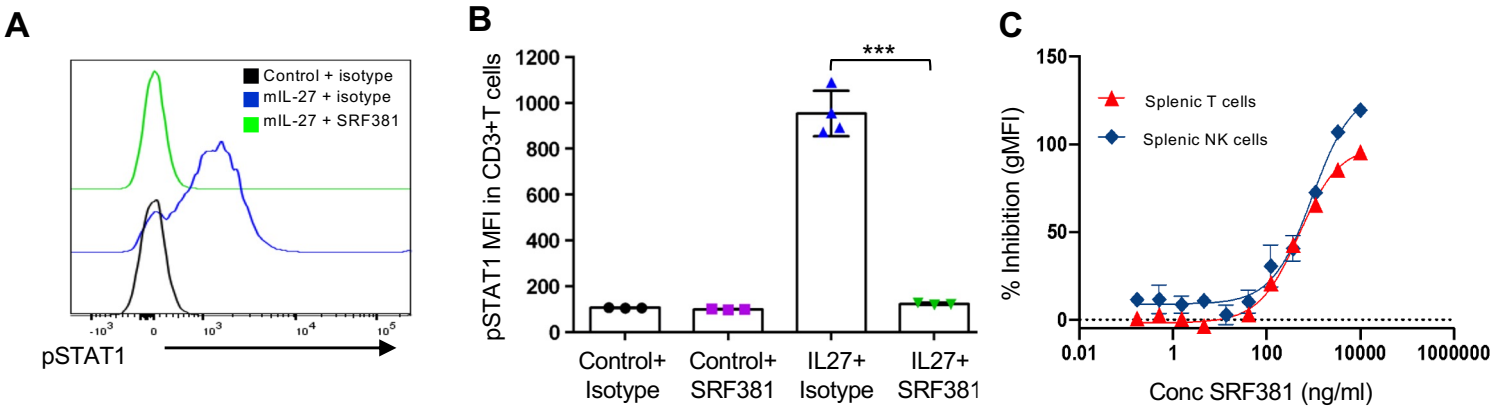

Supplementary Figure S10. Anti-IL27 (SRF381) inhibits IL27-induced phosphorylation of STAT1 in T cells and NK cells. A,B, Mice were injected with empty vector (control) or murine IL27 (mIL27) minicircles to induce ectopic IL27 expression by hydrodynamic transfection. Five days after transfection mice were treated I.P. with 1 mg of either SRF381 or IgG isotype control antibody. Whole blood was collected 24 h after antibody treatment and plasma was prepared. Plasma from antibody treated, minicircle-expressing mice was incubated for 30 min *in vitro* with splenocytes from naive mice. Cells were then fixed and permeabilized for pSTAT1 staining. Flow cytometry analysis was used to detect pSTAT1 in $CD3^+$ T cells. **C,** Splenocytes from naïve mice were incubated with recombinant murine IL27 (40 ng/ml) for 30 min *in vitro* in the presence or absence of varying concentrations of SRF381. Cells were stained for surface CD3 (T cells) or $NK1.1^+$ (NK cells), then fixed, permeabilized, stained for phospho-STAT1 and analyzed by FACS. Data were normalized to the geometric mean fluorescence intensity (gMFI) of IL27 stimulated vs unstimulated conditions, representing 0% and 100% inhibition, respectively.